

# The CMB cold spot under the lens II: Lensing on polarization and cosmic textures footprints

Pedro da Silveira Ferreira,<sup>a,b</sup> Stephen Owusu

<sup>a</sup>Centro Brasileiro de Pesquisas Físicas, 22290-180, Rio de Janeiro, RJ, Brazil

<sup>b</sup>Observatório do Valongo, Universidade Federal do Rio de Janeiro, 20080-090, Rio de Janeiro, RJ, Brazil

E-mail: [dasferreira.pedro@gmail.com](mailto:dasferreira.pedro@gmail.com), [stevenowusu15@yahoo.com.br](mailto:stevenowusu15@yahoo.com.br)

**Abstract.** We present a quadratic lensing estimator that incorporates off-diagonal correlations in both temperature and polarization CMB maps, and is capable of measuring localized lensing profiles with  $< 10''$  average deflection angle at the  $\sim 3\sigma$  level in upcoming Simons observatory (SO) data. The proposed pipeline is agnostic to the underlying mass profile and can probe the subtle signatures of voids, clusters, and topological defects. As a case study and test scenario we focus on a collapsing cosmic texture, a topological defect that has been proposed to explain the CMB Cold Spot. With the forthcoming SO data, we forecast a  $2.8\sigma$  detection if the texture amplitude reaches the current *Planck* 2018  $2\sigma$  limit, and a  $1.8\sigma$  measurement for the best-fit value, which is remarkable given the expected typical lensing angle of  $< 6''$ . As the next-generation CMB surveys will reach  $\ell > 3000$  for polarization, we demonstrate that its inclusion is significant, boosting the estimator's signal-to-noise ratio by  $\sim 50\%$ , and making it a powerful tool, allowing us to recover faint lensing footprints that were previously inaccessible.

**Keywords:** CMB anomalies, CMB cold spot, gravitational lensing

## 1 Introduction

Upcoming ground-based CMB experiments promise a transformative leap beyond *Planck*, delivering arcminute-scale resolution and high-fidelity polarization maps [1, 2]. Among them, the Simons Observatory (SO) will deploy a suite of small- and large-aperture telescopes on Cerro Toco beginning in 2025, targeting noise levels of  $\Delta_T \simeq 2.6 \mu\text{K} \cdot \text{arcmin}$  and beam sizes as small as  $1\text{--}2'$  at 90–280 GHz [1]. These specifications unlock multipoles up to  $\ell > 3000$  in polarization and  $\ell > 4000$  in temperature, whereas *Planck* is noise-dominated for  $\ell \gtrsim 1000$  in polarization and  $\ell \gtrsim 1800$  for temperature [3]. Crucially, high signal-to-noise ratio (S/N) measurements of the EE and TE power spectra enable lensing estimators that combine temperature and polarization, boosting sensitivity to arcsecond-scale lensing effects, and hence to exotic physics that imprints weak yet coherent patterns on the microwave sky.

In this work we introduce a generalized lensing quadratic estimator that exploits both EE and TE+ET non-diagonal correlations, augmenting the standard temperature pipeline presented in [4]. The formalism is agnostic to the underlying mass distribution, and capable of measuring lensing profiles with  $\lesssim 10''$  typical deflection angles, as expected from compact sources such as clusters, voids and, central to this study, collapsing cosmic textures, with high significance ( $\sim 3\sigma$ ) using SO data.

Our science target for the estimator is the Cosmic Microwave Background (CMB) Cold Spot (CS). The CS is a region in the CMB that appears significantly colder than the surrounding areas, deviating from the expected isotropic distribution predicted by the standard model of cosmology. It is located at galactic coordinate  $(l, b) \sim (209^\circ, 57^\circ)$  and extends approximately  $10^\circ$  in angular radius, see Figure 1. Since its initial identification in the WMAP data [5], the anomaly has been the subject of numerous analyses [6–8]. Observations from the *Planck* satellite reaffirmed the cold spot and placed its significance at roughly  $3\sigma$  when evaluated against the predictions of the  $\Lambda\text{CDM}$  model [9]. Unlike random Gaussian fluctuations predicted by the standard cosmological model  $\Lambda\text{CDM}$ , the CS exhibits a coherent temperature profile that is difficult to attribute to random fluctuations [10, 11].

The possibility that the CS can be explained by Galactic foregrounds is small, as its spectrum remains constant with frequency, and it lies in a region with minimal foreground contamination [12]. However, recently [13] presented evidence that the CMB cold spot could be largely attributable to foreground effects from galaxies, especially those within the Eridanus supergroup. Similarly, the Sunyaev-Zel'dovich effect is an unlikely cause, given the absence of any major low-redshift clusters in that direction. Several alternative explanations have been proposed, such as cosmic texture or huge voids in the line of sight. However, [4] ruled out the possibility that the CS is due to a large void between us and the surface of last scattering. The evidence ratio favored the standard  $\Lambda\text{CDM}$  model over the supervoid hypothesis, with odds of 1:13 (1:20) for SMICA (NILC) maps [14], compared to the original odds 56:1 (21:1) using temperature data alone.

Here we focus on the possibility that the CS is caused by a collapsing cosmic texture. In the early universe, at extraordinarily high energy ( $\sim 10^{15}\text{--}10^{16}$  GeV), it is hypothesized that all fundamental forces, excluding gravity, were unified under a single framework referred to as the Grand Unified Theory (GUT). This theory is described by a larger symmetry group, such as SU(5), SU(10), among others [16, 17]. As the universe expands and cools, it undergoes phase transition leading to the separation of these forces in a process known as spontaneous symmetry breaking [17, 18]. These transitions can lead to the formation of topological defects, including cosmic textures, unstable structures that easily collapse, inducing a perturbation

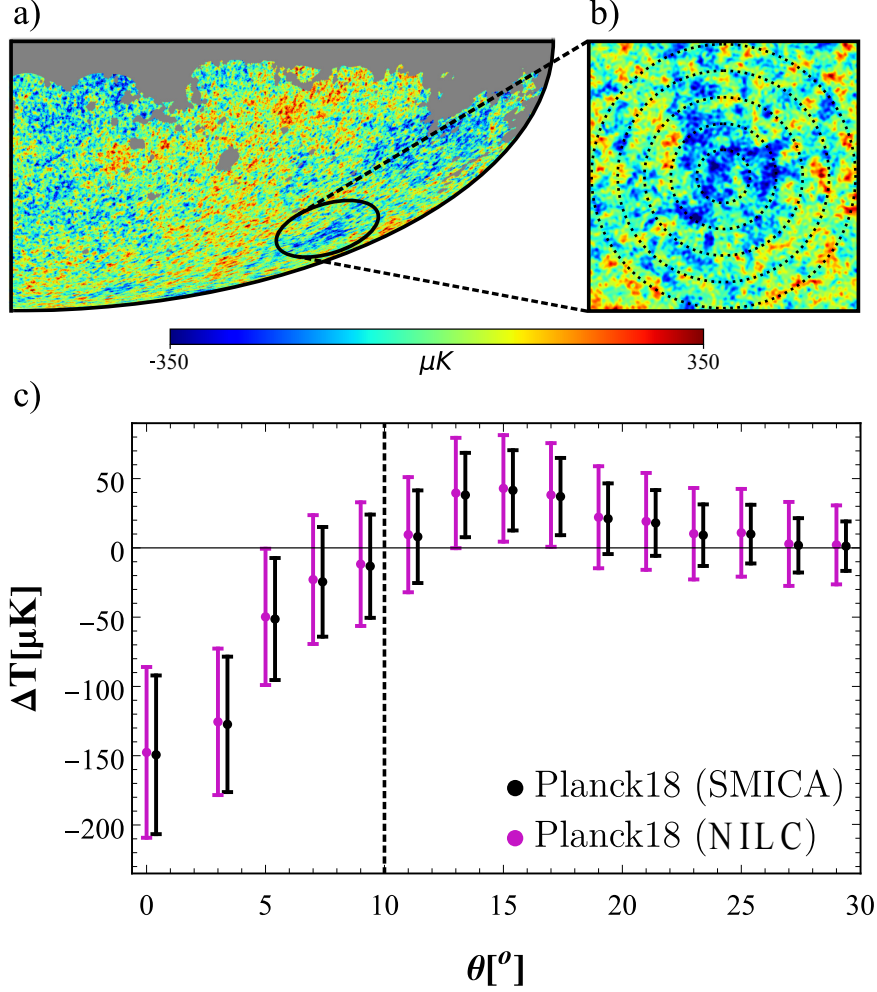


**Figure 1:** **a)** Bottom right quadrant of the *Planck* 2018 CMB temperature map (SMICA pipeline [14]) in Mollweide projection. The colors indicate the temperature variations around the mean. The black ellipse represents the region of the CS. **b)** The CS region zoomed. The plot spans an area of  $10^\circ \times 10^\circ$ . The space between dashed circles indicates the rings of  $2^\circ$  width used to compute the CS temperature profile. **c)** The temperature profile obtained by averaging the pixels inside these rings up to  $\theta = 30^\circ$  for two different component separation pipelines (SMICA and NILC). The dashed line represents the region of the plot b). The error bars are the standard deviation of each ring computed using DX12 *Planck* simulations [15].

in the metric of spacetime that serves as a seed for large-scale structure formation [19]. These perturbations affect the path of photons, resulting in anisotropies, that can register a characteristic hot and cold spots on the CMB.

In addition to the temperature shift, the lensing of the CMB photons caused by the gravitational field generated by the collapsing texture has also been studied [20, 21]. Such lensing has been shown to introduce correlations in the non-diagonal two-point and three-point functions [22, 23]. However, the expected lensing angle for a texture capable of generating the CS is  $\sim 50$  times less than that produced by a void. Another approach to check for the presence of a cosmic texture is to compare the anisotropy profile in both temperature and polarization

maps [24]. Given the tenuous footprint of such an effect, any S/N increment and alternative independent methods should be considered.

In anticipation of the improvements from the incoming new CMB experiments, offering maps with significantly higher angular resolution and precision than the *Planck* Satellite, we introduce our new estimator for polarization, a tool capable of measuring this subtle profile in the foreseen future. We aim to provide the expected lensing S/N that the SO facility can achieve with our method for the measurement of a cosmic texture. Because the formalism makes no assumption about the underlying lens morphology, except by circular symmetry, the same pipeline can be deployed to discover, or constrain, any localized lensing imprint in the CMB maps.

## 2 The cold spot due to a cosmic texture

When CMB photons pass through the non-static gravitational potential of a collapsing texture its temperature is either decreased (redshifted) or increased (blueshifted) depending on whether the photon passed through before or after the collapse [25]. To generate a CS, there should be a temperature decrement via a non-linear Sachs-Wolfe effect (Rees Sciama effect) and this can be approximated by the equations [21, 26]:

$$\frac{\Delta T}{T}(\theta) = \begin{cases} -\epsilon \frac{1}{\sqrt{1 + 4\frac{\theta^2}{\theta_T^2}}} & \theta \leq \theta_*, \\ -\frac{\epsilon}{2} e^{-(\theta^2 - \theta_*^2)/2\theta_T^2} & \theta \geq \theta_*, \end{cases} \quad (2.1)$$

where  $\theta$  is the angle between the observed direction and the structure center, the amplitude is  $\epsilon = 8\pi^2 G \psi_0^2$ , with  $\psi_0$  being the energy scale of symmetry breaking and  $\theta_* \equiv \sqrt{3} \theta_T/2$ . The definition of the scale parameter  $\theta_T$  is

$$\theta_T = \frac{2\sqrt{2}k(1+z_T)}{E(z_T) \int_0^{z_T} \frac{d\bar{z}}{E(\bar{z})}}, \quad (2.2)$$

$k$  is a constant constrained by texture simulations, which suggest a value  $\sim 0.1$  [20, 27],  $z_T$  is the redshift of the texture's centre, and  $E(z) = (\Omega_m(1+z)^3 + \Omega_\Lambda)^{1/2}$ .

The texture not only reduces the temperature of the photons, but also changes the light path, i.e. introducing a lensing signal. While void lensing acts as a diverging lens, the texture converges the photons by the lens profile computed by [28]. However, the results from [28] consider an approximation valid only for angles up to  $\theta \approx \theta_T$ . To obtain a profile applicable at larger angular distances, we followed [10, 21] to extend the profile from its half-maximum following a Gaussian function:

$$\alpha(\theta) = \begin{cases} \frac{2\sqrt{2}\epsilon}{\theta_T} \frac{D_{LS}}{D_S} \frac{\theta}{\sqrt{1 + 4(\theta/\theta_T)^2}}, & \theta \leq \theta_*, \\ \frac{\sqrt{2}\epsilon}{\theta_T} \frac{D_{LS}}{D_S} \theta \exp[-(\theta^2 - \theta_*^2)/(2\theta_T^2)], & \theta > \theta_*, \end{cases} \quad (2.3)$$

with  $D_S$  and  $D_{LS}$  being the comoving distances of the source to the observer and to the lens, respectively. This extension ensures the continuity of both the profile and its first derivative.

## 2.1 Temperature estimator

For the temperature fit we use the following  $\chi^2$  as a function of  $\epsilon$  and  $\theta_T$ :

$$\chi^2(\epsilon, \theta_T) = \sum_i \left[ \frac{\Delta T^{\text{TH}}(\epsilon, \theta_T) - \Delta T^{\text{OBS}}(\theta_i)}{\sigma_{\Delta T^{\text{OBS}}(\theta_i)}} \right]^2. \quad (2.4)$$

We compare the average temperature of a  $2^\circ$  wide ring  $\Delta T^{\text{OBS}}(\theta_i)$ , using the full-resolution SMICA map, centred at  $\theta_i$  (as per Figure 1), with the expected given texture temperature profile model  $\Delta T^{\text{TH}}(\epsilon, \theta_T)$ . We also take into account the uncertainty from observational data  $\sigma_{\Delta T^{\text{OBS}}(\theta_i)}$ . Considering equation 2.1, we obtained the temperature constrained results for Planck 2018 data, see Figure 2.

We estimate  $\epsilon = 6.25_{-3.71}^{+1.75} \times 10^{-5}$  and  $\theta_T = 4.1_{-1.7}^{+2.9}^\circ$ , using the priors  $\epsilon \in [1, 10] \times 10^{-5}$  and  $\theta_T \in [1^\circ, 15^\circ]$ , and considering  $z_T \sim 6$  as a good approximation for the center of the texture [21, 26]. One could, of course, treat  $z_T$  as a free parameter and vary  $D_{LS}$  and  $D_S$  in the estimator; however, for this first forecast we set  $z_T$  fixed. From this point on we fix  $\theta_T$  to its best-fit value obtained above, and we evaluate the S/N after marginalising over  $\epsilon$  within its  $\pm 1\sigma$  and  $\pm 2\sigma$  ranges.

## 3 Lensing effect in CMB polarization maps

We can generalize the temperature derivation in [4, 23] to consider polarization measurement. Here we investigate EE and ET components. Quantitatively, an estimator can be constructed by defining the quantity

$$f_{\ell_1 \ell_2 m} \equiv \frac{1}{2} (a_{\ell_1 m}^* a_{\ell_2 m} + a_{\ell_1 m} a_{\ell_2 m}^*), \quad (3.1)$$

in this case, the coefficient  $a_{\ell m}$  already includes the lensed signal, which is  $a_{\ell m}^{(\text{P})}$ , the unlensed (primordial) signal, plus  $a_{\ell m}^{(\text{L})}$ , the lensing correction ( $a_{\ell m}^{(\text{P})} + a_{\ell m}^{(\text{L})}$ ). It then follows that

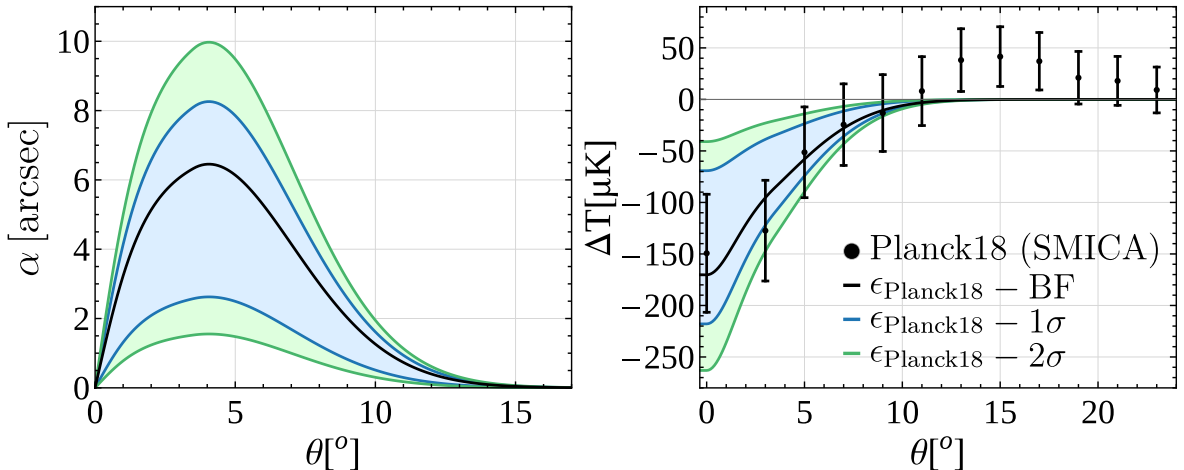


**Figure 2: Left:** Expected lensing angle profile ( $\alpha$ ) in arcseconds for the estimated  $\epsilon$  and  $\theta_T$ , best fit (BF), using *Planck* 18 (SMICA) data and the  $\pm 1\sigma$  and  $\pm 2\sigma$  regions. **Right:** The observed and expected temperature profile considering the same texture parameters.

theoretical non-diagonal two point correlation quantity to first order is given by

$$\begin{aligned}
f_{\ell_1 \ell_2 m}^{TH(E E)} &= \langle a_{\ell_1 m_1}^{EE} a_{\ell_2 m_2}^{EE(L_1)*} \rangle + \langle a_{\ell_1 m_1}^{EE*} a_{\ell_2 m_2}^{EE(L_1)} \rangle \\
&= \frac{(-1)^m}{2} \sum_{\ell_3} {}^2G_{\ell_1 \ell_2 \ell_3}^{-mm0} (1 + (-1)^L) \left( C_{\ell_1}^{EE} \frac{\ell_1(\ell_1 + 1) - \ell_2(\ell_2 + 1) + \ell_3(\ell_3 + 1)}{2} + \right. \\
&\quad \left. C_{\ell_2}^{EE} \frac{\ell_2(\ell_2 + 1) - \ell_1(\ell_1 + 1) + \ell_3(\ell_3 + 1)}{2} \right) b_{\ell_3 0}.
\end{aligned} \tag{3.2}$$

Here, we have used the fact that, for a primordial isotropic and Gaussian signal, the two-point correlation functions take the form:  $\langle a_{\ell_1 m_1}^{(EE)} a_{\ell_2 m_2}^{(EE)*} \rangle = \delta_{\ell_1 \ell_2} \delta_{m_1 m_2} C_{\ell_1}^{(EE)}$ . The Kronecker deltas make it diagonal in the m index. Further, properties of the Gaunt integrals imply that the term with  $\ell_1 = \ell_2$  cancels out entirely [22]. All the signal therefore arises from the off-diagonal modes  $\ell_1 \neq \ell_2$ , although each individual coupling is weak, their broad range still yields a statistically significant contribution. It was shown in [4] that most of the signal is contained in  $|\ell_1 - \ell_2| \equiv \Delta\ell \leq 40$ . We therefore adopt this range for our lensing estimator as a good compromise between computational time and accuracy.

Similarly, for the cross correlations between T and E observables we have

$$\begin{aligned}
f_{\ell_1 \ell_2 m}^{TH,ET} &= \langle a_{\ell_1 m_1}^{ET} a_{\ell_2 m_2}^{ET(L_1)*} \rangle + \langle a_{\ell_1 m_1}^{ET*} a_{\ell_2 m_2}^{ET(L_1)} \rangle \\
&= \frac{(-1)^m}{2} C_{\ell_2}^{ET} \sum_{\ell_3} {}^2G_{\ell_1 \ell_2 \ell_3}^{-mm0} (1 + (-1)^L) \frac{\ell_2(\ell_2 + 1) - \ell_1(\ell_1 + 1) + \ell_3(\ell_3 + 1)}{2} b_{\ell_3 0} + \\
&\quad (-1)^m C_{\ell_1}^{ET} \sum_{\ell_3} {}^0G_{\ell_1 \ell_2 \ell_3}^{-mm0} \frac{\ell_1(\ell_1 + 1) - \ell_2(\ell_2 + 1) + \ell_3(\ell_3 + 1)}{2} b_{\ell_3 0},
\end{aligned} \tag{3.3}$$

with  $L = \ell_1 + \ell_2 + \ell_3$  and where the related spin-2 and spin-0 Gaunt integrals are respectively given as

$${}^2G_{\ell_1 \ell_2 \ell_3}^{-mm0} = \sqrt{\frac{(2\ell_1 + 1)(2\ell_2 + 1)(2\ell_3 + 1)}{4\pi}} \begin{pmatrix} \ell_1 & \ell_2 & \ell_3 \\ 2 & -2 & 0 \end{pmatrix} \begin{pmatrix} \ell_1 & \ell_2 & \ell_3 \\ -m & m & 0 \end{pmatrix}, \tag{3.4}$$

and

$${}^0G_{\ell_1 \ell_2 \ell_3}^{-mm0} = \sqrt{\frac{(2\ell_1 + 1)(2\ell_2 + 1)(2\ell_3 + 1)}{4\pi}} \begin{pmatrix} \ell_1 & \ell_2 & \ell_3 \\ 0 & 0 & 0 \end{pmatrix} \begin{pmatrix} \ell_1 & \ell_2 & \ell_3 \\ -m & m & 0 \end{pmatrix}. \tag{3.5}$$

We have shown the complete derivation for 3.2 and 3.3 in Appendix A and C respectively. See [4, 22, 23] for the TT cross correlations and variance derivation.

The  $b_{\ell m}$  can be defined in terms of a normalized lensing profile  $p(\theta)$  and the amplitude  $\Theta_0$  as done in [4],

$$b_{\ell 0} \equiv 2\pi\Theta_0 \int d\theta \sin \theta p(\theta) Y_{\ell 0}(\theta), \tag{3.6}$$

for convenience we can write  $\hat{b}_{\ell 0} \equiv b_{\ell 0}/\Theta_0$ , where the  $\Theta_0$  is the maximum value of the lensing potential  $\Theta(\theta)$ <sup>1</sup>, related to  $\alpha(\theta)$  as

$$\Theta(\theta) = \int_0^\theta \alpha(\bar{\theta}) d\bar{\theta}, \tag{3.7}$$

---

<sup>1</sup>We consider a lensing profile with circular symmetry, as it only depends on  $\theta$ .

The variances of  $f_{\ell_1\ell_2m}^{\text{TH},\text{XY}}$ , for  $X, Y = \{\text{T}, \text{E}\}$  is given as  $\sigma_{f_{\ell_1\ell_2m}^{\text{TH},\text{XY}}}^2 = \frac{1}{2}C_{\ell_1}^{\text{XY}}C_{\ell_2}^{\text{XY}}(1 + \delta_{m0})$  (see [B](#) and [D](#) for full derivation of EE and TE variances and [\[4\]](#) for the TT variance), one can obtain the corresponding S/N as:

$$\left(\frac{S}{N}\right)_{\text{XY}}^2 = (2 - \delta_{m0}) \sum_{\ell_1, \ell_2, m} \frac{[f_{\ell_1\ell_2m}^{\text{TH},\text{XY}}]^2}{C_{\ell_1}^{(\text{XY})}C_{\ell_2}^{(\text{XY})}}, \quad (3.8)$$

### 3.1 Lensing estimator

Here we present our non-diagonal lensing correlation estimator, which we adjusted for the case of interest, to measure the texture parameters  $\epsilon$  and  $\theta_T$ :

$$\chi_{\text{XY}}^2(\epsilon, \theta_T) = (2 - \delta_{m0}) \sum_{\ell_1=2}^{\ell_{\text{max}}} \sum_{\ell_2=\ell_1+1}^{\ell_1+\Delta\ell} \sum_{m=0}^{\ell_1} \frac{[f_{\ell_1\ell_2m}^{\text{OBS},\text{XY}} - f_{\ell_1\ell_2m}^{\text{TH},\text{XY}}(\epsilon, \theta_T)]^2}{C_{\ell_1}^{\text{XY}}C_{\ell_2}^{\text{XY}}}, \quad (3.9)$$

where  $f_{\ell_1\ell_2m}^{\text{OBS},\text{XY}}$  is the observed non-diagonal two point correlation defined by equation [3.1](#).

## 4 Forecast for Simons observatory

To provide a forecast for the Simons experiment considering both temperature and polarization lensing, we computed [3.8](#) with the texture lensing profile. For this estimation, we considered the specifications provided for the updated optimal case of the Simons Observatory Large Aperture Telescope Survey [\[1\]](#), as in [Table 1](#). This means a co-added noise level of  $2.6 \mu\text{K} \cdot \text{arcmin}$  for temperature, i.e. considering the combination of all frequencies, over the new observed fraction of the sky ( $f_{\text{sky}}$ ) of 61%.

Frequency [GHz]	FWHM [arcmin]	Goal Depth [ $\mu\text{K} \cdot \text{arcmin}$ ]
27	7.4	44
39	5.1	23
93	2.2	3.8
145	1.4	4.1
225	1.0	10
280	0.9	25

**Table 1:** Anticipated instrumental specifications and map-depth characteristics for the full nine-year SO LAT survey (2025–2034) as per [\[1\]](#).

The noise power spectrum was thus achieved by

$$N_\ell = \left[ \sum_{i=1}^{\#\text{freqs}} \left( \sigma_{\theta,i}^2 \sigma_{T,i}^2 \exp \left[ \frac{\ell(\ell+1)\theta_i^2}{8 \log 2} \right] \right)^{-2} \right]^{-1/2}. \quad (4.1)$$

Where  $\sigma_{\theta,i}$  is the FWHM of the frequency  $i$  and  $\sigma_{T,i}$  is the depth, or sensitivity, of the frequency. For polarization sensitivity  $\sigma_{P,i}$ , we consider  $\sigma_{P,i} \equiv \sqrt{2}\sigma_{T,i}$ , assuming non-correlated noise between Q and U maps. So, the final power spectrum  $\mathfrak{C}_\ell$  considered is

$$\mathfrak{C}_\ell = \frac{1}{\sqrt{f_{\text{sky}}}}(C_\ell + N_\ell). \quad (4.2)$$



Taking into account this we considered the maximum  $\ell$  ( $\ell_{max}$ ) to be 4250 for TT and TE+ET and 3350 for EE, as we could not retrieve any signal for higher  $\ell$ 's with our estimator. Also, we limited  $\Delta\ell = 37$  as further non-diagonal correlations do not provide noticeable improvement for the given lensing profile and survey.

Although we considered the mask, as long as it does not hit a significant part of the lensing profile  $p(\theta)$  (which translates into the harmonic space as the  $b_{\ell 0}$ ), it will not substantially affect the S/N. This means that if the mask is more than  $\sim 20^\circ$  from the center of the cold spot, it will not cause much reduction to our estimator. A mask can affect the signal slightly as it introduces non-diagonal correlations that can attenuate the expected lensing footprint. However, it is still a subtle effect, as we tested with realistic simulations done for our previous work [4].

In light of our estimator and the survey specifications provided, the estimated S/N for TT, EE, TE + ET and the total lensing signal using Planck constraints for  $\epsilon$  and  $\theta_T$  is given in Figure 3.

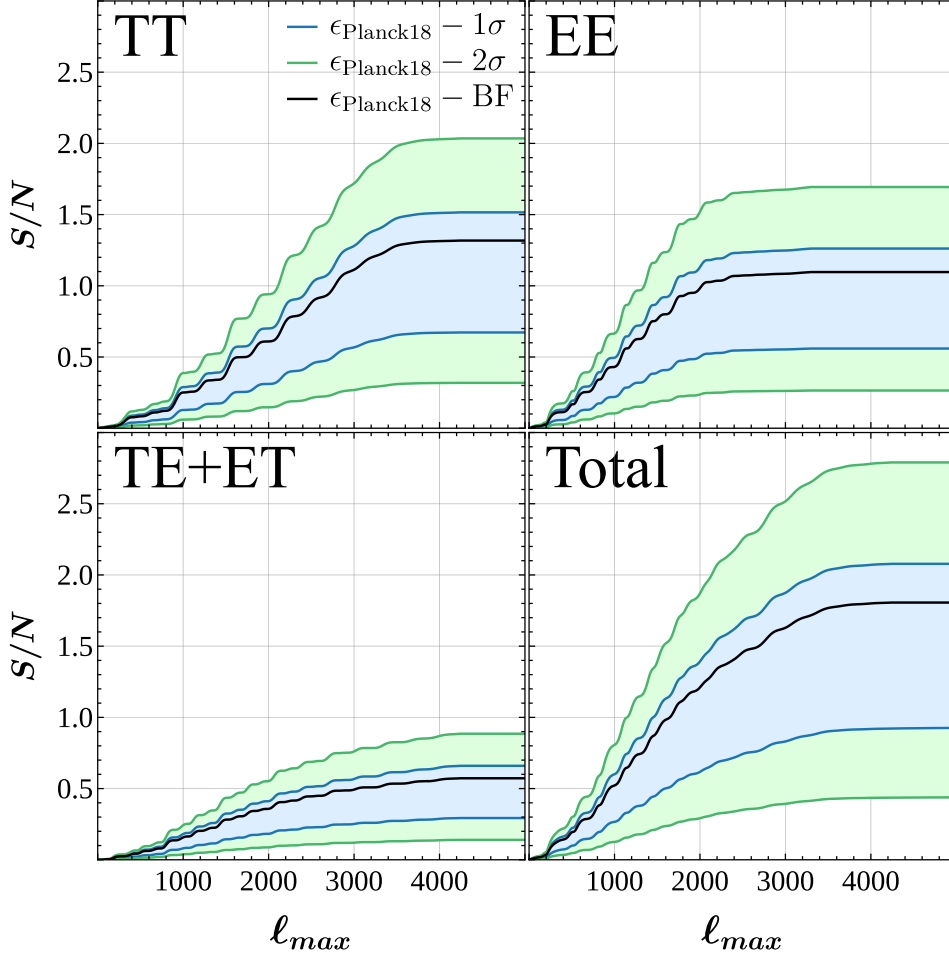


**Figure 3:** Expected signal-to-noise ratio (S/N) for the lensing signal in Simons Observatory data using our estimator on TT, EE, TE+ET and combined (Total, TT+EE+TE+ET) data. We consider the best fit (BF)  $\epsilon$  and  $\theta_T$ , and the  $\pm 1\sigma$  and  $\pm 2\sigma$  bounds for  $\epsilon$  texture parameter obtained using *Planck* 18 (SMICA) data [14]. The Simons Observatory is expected to detect lensing signatures with mean deflection angles of  $\leq 10$  arcsec at high significance ( $2.8\sigma$ ).



For the optimal scenario, the  $2\sigma$  upper limit for the  $\epsilon$  parameter from the *Planck* 2018 data, we expect to be able to measure the texture lensing signature with  $2.8\sigma$  significance when combining temperature and polarization. This means that the Simons Observatory will be able to detect with high significance a lensing profile with an average deflecting angle less than  $\sim 10''$ . Considering only the temperature map, we can obtain in the same optimistic case a  $2\sigma$  detection, while EE provides  $1.7\sigma$  and  $0.9\sigma$  for the crossed TE+ET signal. For the best-fit texture parameters, the expected total S/N is 1.8, which is still impressive given the  $\leq 6$  arcsec lensing angle estimated typical deflecting angle. These constraints are limited by the precision of  $\epsilon$  and  $\theta_T$  measurements using *Planck* 2018 data [14].

## 5 Conclusions and Perspectives

Cosmic textures constitute a unique messenger from the very early universe, tracing physics at energy scales of  $10^{15} - 10^{16}$  GeV characteristic of Grand Unified Theories (GUTs)[19]. Their imprints on the CMB therefore encode information from an era earlier than photon decoupling and, potentially, earlier than inflation itself, providing an observational handle on GUT-scale physics that is otherwise inaccessible to laboratory experiments or lower-energy cosmological probes [19, 28–30]. Detecting (or tightly constraining) a texture signature would thus illuminate the structure of the primordial universe and place direct limits on high-energy particle models far beyond the reach of colliders.

All things considered, the lensing signal from a texture capable of producing the CS could be detected at high significance,  $2.8\sigma$  with the Simons Observatory, provided the optimistic scenario in which the texture amplitude equals the  $2\sigma$  upper-bound constraint derived from *Planck* 2018 data [14]. Taking into account the best-fit scenario, the S/N is reduced to only 1.8, yet a remarkable sensitivity given the expected bending of no more than 6 arcsec. Adding polarization proves crucial: relative to a temperature-only reconstruction, the inclusion of polarization improves the cumulative S/N by  $\sim 50\%$ , allowing the detection of lensing signals that were previously beyond reach.

Nevertheless, the methodology introduced here provides a powerful means of detecting subtle lensing signatures, at the  $\sim 10''$  level, in forthcoming Simons Observatory data. Although a topological defect served as our case study, the pipeline is agnostic: it can be applied to any lensing profile and its corresponding temperature (or polarization) signature.

Although *Planck* polarization is noise-dominated beyond  $\ell > 1000$  [3], next-generation surveys will reach  $\ell > 3000$  and substantially increase the S/N of lensing estimators by incorporating polarization, crucial for detecting the weak signatures from voids, clusters, and topological defects with our method.

Looking several decades ahead, a next-generation facility, such as the proposed CMD-HD [31], with an exquisite limit of  $\ell \sim 25000$ , could detect even dimmer phenomena. With that angular resolution, the experiment will push the sensitivity frontier to phenomena an order of magnitude fainter than those accessible today, enabling direct detection of the Kaiser–Stebbins effect and lensing imprint from cosmic strings, whose characteristic lensing deflection scale is  $\lesssim 1''$  [32].

By combining all the lensing imprints present in the CMB maps, we can now look for fainter remnants of the primordial universe. The proposed estimator can be used as a new promising tool to put not only the cold spot under the lens, but to investigate any lensing footprints on CMB data, now taking advantage of the full set of evidence, i.e, temperature and polarization.

## A The $F_{\ell_1 \ell_2 m}^{EE}$ component

As it was done in temperature [4, 22, 23], we decompose the polarization in the spherical harmonic [33]

$$_{\pm}X(\hat{n}) = \sum_{\ell m} _{\pm}X_{\ell m \pm 2} Y_{\ell}^m(\hat{n}), \quad (\text{A.1})$$

where  $_{\pm}X$  is a complex Stokes parameter given as

$$_{\pm}X = Q(\hat{n}) \pm iU(\hat{n}), \quad (\text{A.2})$$

which is a spin-2 object. Through parity transformation  $_S Y_{\ell}^m \rightarrow (-1)^{\ell} _S Y_{\ell}^m$ , we introduce the parity eigenstates [34]

$$_{\pm}X_{\ell m} = E_{\ell m} \pm iB_{\ell m}, \quad (\text{A.3})$$

such that  $E(\hat{n})$  and  $B(\hat{n})$  are real scalar quantities, with positive  $((-1)^{\ell})$ , “electric” and negative  $((-1)^{\ell+1})$ , “magnetic” parity respectively, given as:

$$E(\hat{n}) = \sum_{\ell m} a_{\ell m}^E Y_{\ell}^m(\hat{n}), \quad a_{\ell m}^E = -\frac{a_{2\ell m} + a_{-2\ell m}}{2}, \quad (\text{A.4})$$

$$B(\hat{n}) = \sum_{\ell m} a_{\ell m}^B Y_{\ell}^m(\hat{n}), \quad a_{\ell m}^B = i\frac{a_{2\ell m} - a_{-2\ell m}}{2}. \quad (\text{A.5})$$

The weak lensing effect induces off-diagonal correlations in harmonic space, as characterized by the two-point function derived in [33], which remaps the primordial anisotropy according to  $b_{\ell m}$  as follows:

$$_{\pm}\tilde{X}_{\ell m} = _{\pm}X_{\ell m} + \sum_{\ell_1 m_1} \sum_{\ell_2 m_2} b_{\ell_1 m_1 \pm 2} X_{\ell_2 m_2 \pm 2} I_{\ell \ell_1 \ell_2}^{mm_1 m_2}, \quad (\text{A.6})$$

where we have considered only up to the first order term in  $b_{\ell m}$ , and the geometrical factor expressed now as integrals over the spin-2 harmonics

$$_{\pm 2}I_{\ell \ell_1 \ell_2}^{mm_1 m_2} = \int d\hat{n} _{\pm 2}Y_{\ell}^{m*}(\nabla_i Y_{\ell_1}^{m_1})(\nabla^i _{\pm 2}Y_{\ell_2}^{m_2}), \quad (\text{A.7})$$

Substituting equation (A.3) into equation (A.6) we get

$$_{\pm}\tilde{X}_{\ell m} = _{\pm}X_{\ell m} + \sum_{\ell_1 m_1} \sum_{\ell_2 m_2} b_{\ell_1 m_1 \pm 2} (E_{\ell m} \pm iB_{\ell m}) _{\pm 2}I_{\ell \ell_1 \ell_2}^{mm_1 m_2}. \quad (\text{A.8})$$

Using the spin-2 angular Laplacian of a tensor

$$\nabla^2 _{\pm 2}Y_{\ell}^m = [-\ell(\ell+2) + 4] _{\pm 2}Y_{\ell}^m, \quad (\text{A.9})$$

we can write

$$_{\pm 2}I_{\ell \ell_1 \ell_2}^{mm_1 m_2} = \frac{1}{2}[\ell_1(\ell_1+1) + \ell_2(\ell_2+1) - \ell(\ell+1)] \int d\hat{n} _{\pm 2}Y_{\ell}^{m*}(\nabla_i Y_{\ell_1}^{m_1})(\nabla^i _{\pm 2}Y_{\ell_2}^{m_2}), \quad (\text{A.10})$$

leading to

$$\begin{aligned} \pm 2 I_{\ell_1 \ell_2}^{mm_1 m_2} &= \frac{1}{2} [\ell_1(\ell_1 + 1) + \ell_2(\ell_2 + 1) - \ell(\ell + 1)] \sqrt{\frac{(2\ell_1 + 1)(2\ell_2 + 1)(2\ell + 1)}{4\pi}} \times \\ &\quad \begin{pmatrix} \ell_1 & \ell_2 & \ell_3 \\ 2 & 0 & -2 \end{pmatrix} \begin{pmatrix} \ell_1 & \ell_2 & \ell_3 \\ -m_1 & m_2 & m \end{pmatrix} (-1)^{m_1+2}. \end{aligned} \quad (\text{A.11})$$

We can write the scalar in terms of the spherical harmonic as

$$E = \frac{1}{2} ({}_2X_{\ell m} + {}_{-2}X_{\ell m}) \quad \text{and} \quad B = \frac{i}{2} ({}_2X_{\ell m} - {}_{-2}X_{\ell m}), \quad (\text{A.12})$$

this can help us express the power EE component as well as the cross spectrum between  $E$  and  $T$ .

$$\langle \tilde{E}_{\ell m} \tilde{E}_{\ell' m'}^* \rangle = \frac{1}{4} [{}_2\tilde{X}_{\ell m} {}_2\tilde{X}_{\ell' m'}^* + {}_{-2}\tilde{X}_{\ell m} {}_{-2}\tilde{X}_{\ell' m'}^* + {}_{-2}\tilde{X}_{\ell m} \tilde{X}_{\ell' m'}^* + {}_2\tilde{X}_{\ell m} {}_{-2}\tilde{X}_{\ell' m'}^*]. \quad (\text{A.13})$$

Again we consider up to the first order terms in lensing,  $b_{\ell m}$ . Taking each term in equation (A.13) we have the following,

$$\begin{aligned} {}_2\tilde{X}_{\ell m} {}_2\tilde{X}_{\ell' m'}^* &= \sum_{\ell_1 m_1} \sum_{\ell_2 m_2} b_{\ell_1 m_1} \langle {}_2X_{\ell_2 m_2} {}_2X_{\ell' m'}^* \rangle {}_2I_{\ell \ell_1 \ell_2}^{mm_1 m_2} \\ &= \sum_{\ell_1 m_1} \sum_{\ell_2 m_2} b_{\ell_1 m_1} (E_{\ell_2 m_2} + iB_{\ell_2 m_2}) (E_{\ell' m'} - iB_{\ell' m'}) {}_2I_{\ell \ell_1 \ell_2}^{mm_1 m_2} \\ &= \sum_{\ell_1 m_1} \sum_{\ell_2 m_2} b_{\ell_1 m_1} (C_{\ell_2}^{EE} + C_{\ell_2}^{BB}) {}_2I_{\ell \ell_1 \ell_2}^{mm_1 m_2} \delta_{\ell_2 \ell'} \delta_{m_2 m'}, \end{aligned} \quad (\text{A.14})$$

$$\begin{aligned} {}_{-2}\tilde{X}_{\ell m} {}_{-2}\tilde{X}_{\ell' m'}^* &= \sum_{\ell_1 m_1} \sum_{\ell_2 m_2} b_{\ell_1 m_1} \langle {}_{-2}X_{\ell_2 m_2} {}_{-2}X_{\ell' m'}^* \rangle {}_{-2}I_{\ell \ell_1 \ell_2}^{mm_1 m_2} \\ &= \sum_{\ell_1 m_1} \sum_{\ell_2 m_2} b_{\ell_1 m_1} (E_{\ell_2 m_2} - iB_{\ell_2 m_2}) (E_{\ell' m'} + iB_{\ell' m'}) {}_{-2}I_{\ell \ell_1 \ell_2}^{mm_1 m_2} \\ &= \sum_{\ell_1 m_1} \sum_{\ell_2 m_2} b_{\ell_1 m_1} (C_{\ell_2}^{EE} - C_{\ell_2}^{BB}) {}_{-2}I_{\ell \ell_1 \ell_2}^{mm_1 m_2} \delta_{\ell_2 \ell'} \delta_{m_2 m'}, \end{aligned} \quad (\text{A.15})$$

$$\begin{aligned} {}_{-2}\tilde{X}_{\ell m} {}_2\tilde{X}_{\ell' m'}^* &= \sum_{\ell_1 m_1} \sum_{\ell_2 m_2} b_{\ell_1 m_1} \langle {}_{-2}X_{\ell_2 m_2} {}_2X_{\ell' m'}^* \rangle {}_{-2}I_{\ell \ell_1 \ell_2}^{mm_1 m_2} \\ &= \sum_{\ell_1 m_1} \sum_{\ell_2 m_2} b_{\ell_1 m_1} (E_{\ell_2 m_2} - iB_{\ell_2 m_2}) (E_{\ell' m'} - iB_{\ell' m'}) {}_{-2}I_{\ell \ell_1 \ell_2}^{mm_1 m_2} \\ &= \sum_{\ell_1 m_1} \sum_{\ell_2 m_2} b_{\ell_1 m_1} (C_{\ell_2}^{EE} - C_{\ell_2}^{BB}) {}_{-2}I_{\ell \ell_1 \ell_2}^{mm_1 m_2} \delta_{\ell_2 \ell'} \delta_{m_2 m'}, \end{aligned} \quad (\text{A.16})$$

$$\begin{aligned} {}_2\tilde{X}_{\ell m} {}_{-2}\tilde{X}_{\ell' m'}^* &= \sum_{\ell_1 m_1} \sum_{\ell_2 m_2} b_{\ell_1 m_1} \langle {}_2X_{\ell_2 m_2} {}_{-2}X_{\ell' m'}^* \rangle {}_2I_{\ell \ell_1 \ell_2}^{mm_1 m_2} \\ &= \sum_{\ell_1 m_1} \sum_{\ell_2 m_2} b_{\ell_1 m_1} (E_{\ell_2 m_2} + iB_{\ell_2 m_2}) (E_{\ell' m'} + iB_{\ell' m'}) {}_2I_{\ell \ell_1 \ell_2}^{mm_1 m_2} \\ &= \sum_{\ell_1 m_1} \sum_{\ell_2 m_2} b_{\ell_1 m_1} (C_{\ell_2}^{EE} + C_{\ell_2}^{BB}) {}_2I_{\ell \ell_1 \ell_2}^{mm_1 m_2} \delta_{\ell_2 \ell'} \delta_{m_2 m'}. \end{aligned} \quad (\text{A.17})$$

Combining all terms and choosing the  $\hat{z}$  axis to point towards the centre of the lensing profile, meaning we can consider  $m_1 = 0$ , we have

$$\langle a_{\ell m}^{EE} a_{\ell' m'}^{EE(L_1)*} \rangle = \frac{1}{2} C_{\ell'}^{EE} \sum_{\ell_1} b_{\ell_1 0} {}_2I_{\ell \ell_1 \ell'}^{m 0 m'} (1 + (-1)^L), \quad (\text{A.18})$$

$$\langle a_{\ell' m'}^{EE*} a_{\ell m}^{EE(L_1)} \rangle = \frac{1}{2} C_{\ell}^{EE} \sum_{\ell_1} b_{\ell_1 0} {}_2I_{\ell' \ell_1 \ell}^{m' 0 m} (1 + (-1)^L), \quad (\text{A.19})$$

where we have used

$${}_{\pm 2}I_{\ell \ell_1 \ell_2}^{mm_1 m_2} = (-1)^L {}_{\mp 2}I_{\ell \ell_1 \ell_2}^{mm_1 m_2}, \quad (\text{A.20})$$

with  $L = \ell + \ell_1 + \ell_2$ . It then follows that theoretical non-diagonal two point correlation quantity is given by:

$$\begin{aligned} f_{l_1 l_2 m}^{TH(E E)} &= \langle a_{\ell_1 m_1}^{EE} a_{\ell_2 m_2}^{EE(L_1)*} \rangle + \langle a_{\ell_1 m_1}^{EE*} a_{\ell_2 m_2}^{EE(L_1)} \rangle \\ &= \frac{(-1)^m}{2} \sum_{\ell_3} {}_2G_{\ell_1 \ell_2 \ell_3}^{-mm 0} (1 + (-1)^L) \left( C_{\ell_1}^{EE} \frac{\ell_1(\ell_1 + 1) - \ell_2(\ell_2 + 1) + \ell_3(\ell_3 + 1)}{2} + \right. \\ &\quad \left. C_{\ell_2}^{EE} \frac{\ell_2(\ell_2 + 1) - \ell_1(\ell_1 + 1) + \ell_3(\ell_3 + 1)}{2} \right) b_{\ell_3 0}, \end{aligned} \quad (\text{A.21})$$

where the related spin-2 Gaunt integral is

$${}_2G_{\ell_1 \ell_2 \ell_3}^{-mm 0} = \sqrt{\frac{(2\ell_1 + 1)(2\ell_2 + 1)(2\ell_3 + 1)}{4\pi}} \begin{pmatrix} \ell_1 & \ell_2 & \ell_3 \\ 2 & 0 & -2 \end{pmatrix} \begin{pmatrix} \ell_1 & \ell_2 & \ell_3 \\ -m & 0 & m \end{pmatrix}. \quad (\text{A.22})$$

## B Variance of $F_{\ell_1 \ell_2 m}^{EE}$

The variance can be defined as  $\sigma_{\ell_1 \ell_2 m}^2 = \langle F_{\ell_1 \ell_2 m}^2 \rangle - \langle F_{\ell_1 \ell_2 m} \rangle^2$ , we then define the necessary quantities as:

$$F_{\ell_1 \ell_2 m}^{EE} \equiv a_{\ell_1 m}^{E*} a_{\ell_2 m}^E, \quad (\text{B.1})$$

$$F_{\ell_1 \ell_2 -m}^{EE} = a_{\ell_1 -m}^{E*} a_{\ell_2 -m}^E, \quad (\text{B.2})$$

where

$$a_{\ell m}^E = a_{\ell m}^{E(P)} + a_{\ell m}^{E(L)}. \quad (\text{B.3})$$

Working with real quantities

$$\frac{1}{2} (F_{\ell_1 \ell_2 m} + F_{\ell_1 \ell_2 -m}) \equiv f_{\ell_1 \ell_2 m}, \quad \frac{1}{2i} (F_{\ell_1 \ell_2 m} - F_{\ell_1 \ell_2 -m}) \equiv g_{\ell_1 \ell_2 m}, \quad (\text{B.4})$$

$$\langle f_{\ell_1 \ell_2 m} f_{\ell'_1 \ell'_2 m'} \rangle = \frac{1}{4} \langle F_{\ell_1 \ell_2 m} F_{\ell'_1 \ell'_2 m'} + F_{\ell_1 \ell_2 m} F_{\ell'_1 \ell'_2 -m'} + F_{\ell_1 \ell_2 -m} F_{\ell'_1 \ell'_2 m'} + F_{\ell_1 \ell_2 -m} F_{\ell'_1 \ell'_2 -m'} \rangle. \quad (\text{B.5})$$

Let us consider the lowest order of diagonal correlation (i.e zero order)

$$F_{\ell_1 \ell_2 m} = a_{\ell_1 m}^{E(P)*} a_{\ell_2 m}^{E(P)} \quad \text{and} \quad F_{\ell_1 \ell_2 -m} = a_{\ell_1 -m}^{E(P)*} a_{\ell_2 -m}^{E(P)}. \quad (\text{B.6})$$

Taking the first part of the variance, we have

$$\begin{aligned} \langle f_{\ell_1 \ell_2 m} f_{\ell'_1 \ell'_2 m'} \rangle_{0th} = & \frac{1}{4} \langle a_{\ell_1 m}^{E*} a_{\ell_2 m}^E a_{\ell'_1 m'}^{E*} a_{\ell'_2 m'}^E \rangle + \frac{1}{4} \langle a_{\ell_1 m}^{E*} a_{\ell_2 m}^E a_{\ell'_1 -m'}^{E*} a_{\ell'_2 -m'}^E \rangle + \\ & \frac{1}{4} \langle a_{\ell_1 -m}^{E*} a_{\ell_2 -m}^E a_{\ell'_1 m'}^{E*} a_{\ell'_2 m'}^E \rangle + \frac{1}{4} \langle a_{\ell_1 -m}^{E*} a_{\ell_2 -m}^E a_{\ell'_1 -m'}^{E*} a_{\ell'_2 -m'}^E \rangle. \end{aligned} \quad (\text{B.7})$$

For simplicity, we have dropped (P) in the above expression and will also be dropped in the subsequent computations. Since  $a_{\ell m}^P$  is Gaussian by definition, then we can follow the definition that

$$E[X_1 X_2 X_3 X_4] = E[X_1 X_2] E[X_3 X_4] + E[X_1 X_3] E[X_2 X_4] + E[X_1 X_4] E[X_2 X_3]. \quad (\text{B.8})$$

Using the above equation, we can decompose each term in equation (B.7) into various configurations. Taking term by term.

**1st term**

$$\begin{aligned} \frac{1}{4} \langle a_{\ell_1 m}^{E*} a_{\ell_2 m}^E a_{\ell'_1 m'}^{E*} a_{\ell'_2 m'}^E \rangle = & \frac{1}{4} \langle a_{\ell_1 m}^{E*} a_{\ell_2 m}^E \rangle \langle a_{\ell'_1 m'}^{E*} a_{\ell'_2 m'}^E \rangle + \frac{1}{4} \langle a_{\ell_1 m}^{E*} a_{\ell'_1 m'}^{E*} \rangle \langle a_{\ell_2 m}^E a_{\ell'_2 m'}^E \rangle \\ & + \frac{1}{4} \langle a_{\ell_1 m}^{E*} a_{\ell'_2 m'}^E \rangle \langle a_{\ell_2 m}^E a_{\ell'_1 m'}^{E*} \rangle, \end{aligned} \quad (\text{B.9})$$

leading to

$$\begin{aligned} \frac{1}{4} \langle a_{\ell_1 m}^{E*} a_{\ell_2 m}^E a_{\ell'_1 m'}^{E*} a_{\ell'_2 m'}^E \rangle = & \frac{1}{4} \delta_{\ell_1 \ell_2} \delta_{\ell'_1 \ell'_2} C_{\ell_1}^{EE} C_{\ell'_2}^{EE} + \frac{1}{4} \delta_{\ell'_2 \ell_2} \delta_{\ell_1 \ell'_1} \delta_{m-m'} C_{\ell_1}^{EE} C_{\ell'_2}^{EE} + \\ & \frac{1}{4} \delta_{\ell_1 \ell'_2} \delta_{\ell_2 \ell'_1} \delta_{mm'} C_{\ell_1}^{EE} C_{\ell'_2}^{EE}, \end{aligned} \quad (\text{B.10})$$

similarly, the other terms in equation B.7 will generate the following respective expressions

$$\begin{aligned} \frac{1}{4} \langle a_{\ell_1 m}^{E*} a_{\ell_2 m}^E a_{\ell'_1 -m'}^{E*} a_{\ell'_2 -m'}^E \rangle = & \frac{1}{4} \delta_{\ell_1 \ell_2} \delta_{\ell'_1 \ell'_2} C_{\ell_1}^{EE} C_{\ell'_2}^{EE} + \frac{1}{4} \delta_{\ell'_2 \ell_2} \delta_{\ell_1 \ell'_1} \delta_{mm'} C_{\ell_1}^{EE} C_{\ell'_2}^{EE} + \\ & \frac{1}{4} \delta_{\ell_1 \ell'_2} \delta_{\ell_2 \ell'_1} \delta_{m-m'} C_{\ell_1}^{EE} C_{\ell'_2}^{EE}, \end{aligned} \quad (\text{B.11})$$

$$\begin{aligned} \frac{1}{4} \langle a_{\ell_1 -m}^{E*} a_{\ell_2 -m}^E a_{\ell'_1 m'}^{E*} a_{\ell'_2 m'}^E \rangle = & \frac{1}{4} \delta_{\ell_1 \ell_2} \delta_{\ell'_1 \ell'_2} C_{\ell_1}^{EE} C_{\ell'_2}^{EE} + \frac{1}{4} \delta_{\ell'_2 \ell_2} \delta_{\ell_1 \ell'_1} \delta_{mm'} C_{\ell_1}^{EE} C_{\ell'_2}^{EE} + \\ & \frac{1}{4} \delta_{\ell_1 \ell'_2} \delta_{\ell_2 \ell'_1} \delta_{-mm'} C_{\ell_1}^{EE} C_{\ell'_2}^{EE}, \end{aligned} \quad (\text{B.12})$$

$$\begin{aligned} \frac{1}{4} \langle a_{\ell_1 -m}^{E*} a_{\ell_2 -m}^E a_{\ell'_1 -m'}^{E*} a_{\ell'_2 -m'}^E \rangle = & \frac{1}{4} \delta_{\ell_1 \ell_2} \delta_{\ell'_1 \ell'_2} C_{\ell_1}^{EE} C_{\ell'_2}^{EE} + \frac{1}{4} \delta_{\ell'_2 \ell_2} \delta_{\ell_1 \ell'_1} \delta_{m-m'} C_{\ell_1}^{EE} C_{\ell'_2}^{EE} + \\ & \frac{1}{4} \delta_{\ell_1 \ell'_2} \delta_{\ell_2 \ell'_1} \delta_{m'm} C_{\ell_1}^{EE} C_{\ell'_2}^{EE}. \end{aligned} \quad (\text{B.13})$$

Using the symmetric condition present in our model,

$$\ell_2 > \ell_1, \ell'_2 > \ell'_1 \quad \text{and} \quad m' = m, \quad (\text{B.14})$$

the variance results in

$$\langle f_{\ell_1 \ell_2 m} f_{\ell'_1 \ell'_2 m'} \rangle_{0th} - \langle f_{\ell_1 \ell_2 m} \rangle \langle f_{\ell'_1 \ell'_2 m'} \rangle_{0th} = \frac{1}{2} \delta_{\ell_2 \ell'_2} \delta_{\ell_1 \ell'_1} C_{\ell_1}^{EE} C_{\ell_2}^{EE} + \frac{1}{2} \delta_{\ell_2 \ell'_2} \delta_{\ell_1 \ell'_1} \delta_{m-m'} C_{\ell_1}^{EE} C_{\ell_2}^{EE}, \quad (\text{B.15})$$

where the second part of the variance can easily be obtained as  $\langle f_{\ell_1 \ell_2 m} \rangle \langle f_{\ell'_1 \ell'_2 m'} \rangle_{0th} = \delta_{\ell_1 \ell_2} \delta_{\ell'_1 \ell'_2} C_{\ell_1}^{EE} C_{\ell'_2}^{EE}$ . Finally we can write the variance as

$$\sigma_{\ell_1 \ell_2 m}^2 = \frac{1}{2} \delta_{\ell_2 \ell'_2} \delta_{\ell_1 \ell'_1} (\delta_{m0} + 1) C_{\ell_1}^{EE} C_{\ell_2}^{EE}. \quad (\text{B.16})$$

## C The $F_{\ell_1 \ell_2 m}^{TE}$ component

For lensed temperature field

$$\tilde{\Theta}_{\ell m} = \Theta_{\ell m} + \sum_{\ell_1 m_1} \sum_{\ell_2 m_2} b_{\ell_1 m_1} \Theta_{\ell_2 m_2} I_{\ell \ell_1 \ell_2}^{m m_1 m_2}, \quad (\text{C.1})$$

in this case, for the temperature, the geometrical factor can be expressed as integrals over the spin-0 harmonics [33]

$$I_{\ell \ell_1 \ell_2}^{m m_1 m_2} = \frac{1}{2} [\ell_1 (\ell_1 + 1) + \ell_2 (\ell_2 + 1) - \ell (\ell + 1)] \sqrt{\frac{(2\ell_1 + 1)(2\ell_2 + 1)(2\ell + 1)}{4\pi}} \times \begin{pmatrix} \ell_1 & \ell_2 & \ell_3 \\ 0 & 0 & 0 \end{pmatrix} \begin{pmatrix} \ell_1 & \ell_2 & \ell_3 \\ -m_1 & m_2 & m \end{pmatrix} (-1)^{m_1}. \quad (\text{C.2})$$

The polarization field is given by equation A.6.

The power ET component is then

$$\langle \tilde{E}_{\ell m} \tilde{\Theta}_{\ell' m'}^* \rangle = \frac{1}{2} {}_2\tilde{X}_{\ell m} \tilde{\Theta}_{\ell' m'}^* + \frac{1}{2} {}_{-2}\tilde{X}_{\ell m} \tilde{\Theta}_{\ell' m'}^*. \quad (\text{C.3})$$

Using the first-order approximation, each term becomes:

$$\begin{aligned} {}_2\tilde{X}_{\ell m} \tilde{\Theta}_{\ell' m'}^* &= \sum_{\ell_1 m_1} \sum_{\ell_2 m_2} b_{\ell_1 m_1} \langle {}_2X_{\ell_2 m_2} \Theta_{\ell' m'}^* \rangle {}_2I_{\ell \ell_1 \ell_2}^{m m_1 m_2} + \\ &\quad \sum_{\ell_1 m_1} \sum_{\ell_2 m_2} b_{\ell_1 m_1} \langle \Theta_{\ell_2 m_2}^* {}_2X_{\ell m} \rangle I_{\ell' \ell_1 \ell_2}^{m' m_1 m_2}, \end{aligned} \quad (\text{C.4})$$

and

$$\begin{aligned} {}_{-2}\tilde{X}_{\ell m} \tilde{\Theta}_{\ell' m'}^* &= \sum_{\ell_1 m_1} \sum_{\ell_2 m_2} b_{\ell_1 m_1} \langle {}_{-2}X_{\ell_2 m_2} \Theta_{\ell' m'}^* \rangle {}_2I_{\ell \ell_1 \ell_2}^{m m_1 m_2} + \\ &\quad \sum_{\ell_1 m_1} \sum_{\ell_2 m_2} b_{\ell_1 m_1} \langle \Theta_{\ell_2 m_2}^* {}_{-2}X_{\ell m} \rangle I_{\ell' \ell_1 \ell_2}^{m' m_1 m_2}. \end{aligned} \quad (\text{C.5})$$

Equivalently the above can be expressed as

$$\pm {}_2\tilde{X}_{\ell m} \tilde{\Theta}_{\ell' m'}^* = \langle a_{\ell' m'}^{E(L_1)*} a_{\ell m}^T \rangle + \langle a_{\ell m}^E a_{\ell' m'}^{T(L_1)*} \rangle. \quad (\text{C.6})$$

Using equation A.3 and we have

$$\begin{aligned}
{}_2\tilde{X}_{\ell m}\tilde{\Theta}_{\ell' m'}^* &= \sum_{\ell_1 m_1} \sum_{\ell_2 m_2} b_{\ell_1 m_1} \langle E_{\ell_2 m_2} \Theta_{\ell' m'}^* \rangle_2 I_{\ell \ell_1 \ell_2}^{mm_1 m_2} + i \sum_{\ell_1 m_1} \sum_{\ell_2 m_2} b_{\ell_1 m_1} \langle B_{\ell_2 m_2} \Theta_{\ell' m'}^* \rangle_2 I_{\ell \ell_1 \ell_2}^{mm_1 m_2} \\
&+ \sum_{\ell_1 m_1} \sum_{\ell_2 m_2} b_{\ell_1 m_1} \langle E_{\ell m} \Theta_{\ell_2 m_2}^* \rangle I_{\ell' \ell_1 \ell_2}^{m' m_1 m_2} + i \sum_{\ell_1 m_1} \sum_{\ell_2 m_2} b_{\ell_1 m_1} \langle B_{\ell m} \Theta_{\ell_2 m_2}^* \rangle I_{\ell' \ell_1 \ell_2}^{m' m_1 m_2},
\end{aligned} \tag{C.7}$$

and

$$\begin{aligned}
-{}_2\tilde{X}_{\ell m}\tilde{\Theta}_{\ell' m'}^* &= \sum_{\ell_1 m_1} \sum_{\ell_2 m_2} b_{\ell_1 m_1} \langle E_{\ell_2 m_2} \Theta_{\ell' m'}^* \rangle_{-2} I_{\ell \ell_1 \ell_2}^{mm_1 m_2} - i \sum_{\ell_1 m_1} \sum_{\ell_2 m_2} b_{\ell_1 m_1} \langle B_{\ell_2 m_2} \Theta_{\ell' m'}^* \rangle_{-2} I_{\ell \ell_1 \ell_2}^{mm_1 m_2} \\
&+ \sum_{\ell_1 m_1} \sum_{\ell_2 m_2} b_{\ell_1 m_1} \langle E_{\ell m} \Theta_{\ell_2 m_2}^* \rangle I_{\ell' \ell_1 \ell_2}^{m' m_1 m_2} - i \sum_{\ell_1 m_1} \sum_{\ell_2 m_2} b_{\ell_1 m_1} \langle B_{\ell m} \Theta_{\ell_2 m_2}^* \rangle I_{\ell' \ell_1 \ell_2}^{m' m_1 m_2}.
\end{aligned} \tag{C.8}$$

Equation C.3 now becomes

$$\begin{aligned}
\langle \tilde{E}_{\ell m} \tilde{\Theta}_{\ell' m'}^* \rangle &= \frac{1}{2} \sum_{\ell_1 m_1} \sum_{\ell_2 m_2} b_{\ell_1 m_1} \langle E_{\ell_2 m_2} \Theta_{\ell' m'}^* \rangle_2 I_{\ell \ell_1 \ell_2}^{mm_1 m_2} + \frac{1}{2} \sum_{\ell_1 m_1} \sum_{\ell_2 m_2} b_{\ell_1 m_1} \langle E_{\ell_2 m_2} \Theta_{\ell' m'}^* \rangle_{-2} I_{\ell \ell_1 \ell_2}^{mm_1 m_2} \\
&+ \sum_{\ell_1 m_1} \sum_{\ell_2 m_2} b_{\ell_1 m_1} \langle E_{\ell m} \Theta_{\ell_2 m_2}^* \rangle I_{\ell' \ell_1 \ell_2}^{m' m_1 m_2} + \frac{1}{2} i \sum_{\ell_1 m_1} \sum_{\ell_2 m_2} b_{\ell_1 m_1} \langle B_{\ell_2 m_2} \Theta_{\ell' m'}^* \rangle_2 I_{\ell \ell_1 \ell_2}^{mm_1 m_2} \\
&- \frac{1}{2} i \sum_{\ell_1 m_1} \sum_{\ell_2 m_2} b_{\ell_1 m_1} \langle B_{\ell_2 m_2} \Theta_{\ell' m'}^* \rangle_{-2} I_{\ell \ell_1 \ell_2}^{mm_1 m_2}.
\end{aligned} \tag{C.9}$$

Using the relation given in equation A.20 we get

$$\begin{aligned}
\langle \tilde{E}_{\ell m} \tilde{\Theta}_{\ell' m'}^* \rangle &= \frac{1}{2} \sum_{\ell_1 m_1} \sum_{\ell_2 m_2} b_{\ell_1 m_1} \langle E_{\ell_2 m_2} \Theta_{\ell' m'}^* \rangle_2 I_{\ell \ell_1 \ell_2}^{mm_1 m_2} (1 + (-1)^L) \\
&+ \sum_{\ell_1 m_1} \sum_{\ell_2 m_2} b_{\ell_1 m_1} \langle E_{\ell m} \Theta_{\ell_2 m_2}^* \rangle I_{\ell' \ell_1 \ell_2}^{m' m_1 m_2} \\
&+ \frac{1}{2} i \sum_{\ell_1 m_1} \sum_{\ell_2 m_2} b_{\ell_1 m_1} \langle B_{\ell_2 m_2} \Theta_{\ell' m'}^* \rangle_2 I_{\ell \ell_1 \ell_2}^{mm_1 m_2} (1 - (-1)^L).
\end{aligned} \tag{C.10}$$

Leading to

$$\begin{aligned}
\langle \tilde{E}_{\ell m} \tilde{\Theta}_{\ell' m'}^* \rangle &= \frac{1}{2} \sum_{\ell_1 m_1} \sum_{\ell_2 m_2} b_{\ell_1 m_1} C_{\ell'}^{ET} {}_2I_{\ell \ell_1 \ell_2}^{mm_1 m_2} (1 + (-1)^L) \delta_{\ell_2 \ell'} \delta_{m_2 m'} \\
&+ \sum_{\ell_1 m_1} \sum_{\ell_2 m_2} b_{\ell_1 m_1} C_{\ell}^{ET} I_{\ell' \ell_1 \ell_2}^{m' m_1 m_2} \delta_{\ell \ell_2} \delta_{m m_2} \\
&+ \frac{1}{2} i \sum_{\ell_1 m_1} \sum_{\ell_2 m_2} b_{\ell_1 m_1} C_{\ell'}^{BT} {}_2I_{\ell \ell_1 \ell_2}^{mm_1 m_2} (1 - (-1)^L) \delta_{\ell' \ell_2} \delta_{m' m_2}.
\end{aligned} \tag{C.11}$$

Combining all terms and choosing the  $\hat{z}$  axis to point towards the centre of the lensing profile, meaning we can consider  $m_1 = 0$ , we have

$$\begin{aligned}
\langle \tilde{E}_{\ell m} \tilde{\Theta}_{\ell' m'}^* \rangle &= \frac{1}{2} C_{\ell'}^{ET} \sum_{\ell_1} b_{\ell_1 0} (1 + (-1)^L) {}_2I_{\ell \ell_1 \ell'}^{m 0 m'} + C_{\ell}^{ET} \sum_{\ell_1} b_{\ell_1 0} I_{\ell' \ell_1 \ell}^{m' 0 m} \\
&+ \frac{i}{2} C_{\ell'}^{BT} \sum_{\ell_1} b_{\ell_1 0} {}_2I_{\ell \ell_1 \ell'}^{m 0 m'} (1 - (-1)^L).
\end{aligned} \tag{C.12}$$



We can rewrite the above equation as

$$\begin{aligned} \langle a_{\ell m}^{ET} a_{\ell' m'}^{ET(L_1)*} \rangle + \langle a_{\ell' m'}^{ET(L_1)*} a_{\ell m}^{ET} \rangle &= \frac{1}{2} C_{\ell'}^{ET} \sum_{\ell_1} b_{\ell_1 0} (1 + (-1)^L) {}_2I_{\ell\ell_1\ell'}^{m0m'} + C_{\ell}^{ET} \sum_{\ell_1} b_{\ell_1 0} {}_1I_{\ell'\ell_1\ell}^{m'0m} \\ &+ \frac{i}{2} C_{\ell'}^{BT} \sum_{\ell_1} b_{\ell_1 0} {}_2I_{\ell\ell_1\ell'}^{m0m'} (1 - (-1)^L), \end{aligned} \quad (C.13)$$

where  $a^{ET(L_1)}$  represent first order lensed  $a_{lm}$ . Dropping the imaginary part, since the B component is negligible results in the two point correlation as follows

$$F_{\ell\ell'm}^{TH(ET)} = \frac{1}{2} C_{\ell'}^{ET} \sum_{\ell_1} b_{\ell_1 0} (1 + (-1)^L) {}_2I_{\ell\ell_1\ell'}^{m0m'} + C_{\ell}^{ET} \sum_{\ell_1} b_{\ell_1 0} {}_1I_{\ell'\ell_1\ell}^{m'0m}. \quad (C.14)$$

Finally we can express the two point correlation quantity as

$$\begin{aligned} F_{\ell_1\ell_2m}^{TH(ET)} &= \frac{(-1)^m}{2} C_{\ell_2}^{ET} \sum_{\ell_3} {}^2G_{\ell_1\ell_2\ell_3}^{-mm0} (1 + (-1)^L) \frac{\ell_2(\ell_2 + 1) - \ell_1(\ell_1 + 1) + \ell_3(\ell_3 + 1)}{2} b_{\ell_3 0} \\ &+ (-1)^m C_{\ell_1}^{ET} \sum_{\ell_3} {}^0G_{\ell_1\ell_2\ell_3}^{-mm0} \frac{\ell_1(\ell_1 + 1) - \ell_2(\ell_2 + 1) + \ell_3(\ell_3 + 1)}{2} b_{\ell_3 0}, \end{aligned} \quad (C.15)$$

where

$${}^0G_{\ell_1\ell_2\ell_3}^{-mm0} = \sqrt{\frac{(2\ell_1 + 1)(2\ell_2 + 1)(2\ell_3 + 1)}{4\pi}} \begin{pmatrix} \ell_1 & \ell_2 & \ell_3 \\ 0 & 0 & 0 \end{pmatrix} \begin{pmatrix} \ell_1 & \ell_2 & \ell_3 \\ -m & m & 0 \end{pmatrix}, \quad (C.16)$$

## D Variance of $F_{\ell_1\ell_2m}^{TE}$

The variance In terms of cross correlation will need the following quantities

$$F_{\ell_1\ell_2m}^{TE} \equiv a_{\ell_1 m}^{T*} a_{\ell_2 m}^E, \quad (D.1)$$

$$F_{\ell_1\ell_2-m}^{TE} = a_{\ell_1 -m}^{T*} a_{\ell_2 -m}^E, \quad (D.2)$$

where

$$a_{\ell m}^T = a_{\ell m}^{T(P)} + a_{\ell m}^{T(L)}, \quad (D.3)$$

and

$$a_{\ell m}^E = a_{\ell m}^{E(P)} + a_{\ell m}^{E(L)}. \quad (D.4)$$

As usual working with real quantities, let us consider the lowest order of diagonal correlation (i.e zero order)

$$F_{\ell_1\ell_2m} = a_{\ell_1 m}^{T(P)*} a_{\ell_2 m}^{E(P)}, \quad (D.5)$$

$$F_{\ell_1 \ell_2 - m} = a_{\ell_1 - m}^{T(P)*} a_{\ell_2 - m}^E, \quad (\text{D.6})$$

$$\begin{aligned} \langle f_{\ell_1 \ell_2 m} f_{\ell'_1 \ell'_2 m'} \rangle_{0th} &= \frac{1}{4} \langle a_{\ell_1 m}^{T*} a_{\ell_2 m}^E a_{\ell'_1 m'}^{T*} a_{\ell'_2 m'}^E \rangle + \frac{1}{4} \langle a_{\ell_1 m}^{T*} a_{\ell_2 m}^E a_{\ell'_1 - m'}^{T*} a_{\ell'_2 - m'}^E \rangle \\ &+ \frac{1}{4} \langle a_{\ell_1 - m}^{T*} a_{\ell_2 - m}^E a_{\ell'_1 m'}^{T*} a_{\ell'_2 m'}^E \rangle + \frac{1}{4} \langle a_{\ell_1 - m}^{T*} a_{\ell_2 - m}^E a_{\ell'_1 - m'}^{T*} a_{\ell'_2 - m'}^E \rangle. \end{aligned} \quad (\text{D.7})$$

Similarly, using the Gaussian definition (B.8) we can decompose each term in equation (D.7) into various configurations. Taking term by term.

**1st term**

$$\begin{aligned} \frac{1}{4} \langle a_{\ell_1 m}^{T*} a_{\ell_2 m}^E a_{\ell'_1 m'}^{T*} a_{\ell'_2 m'}^E \rangle &= \frac{1}{4} \langle a_{\ell_1 m}^{T*} a_{\ell_2 m}^E \rangle \langle a_{\ell'_1 m'}^{T*} a_{\ell'_2 m'}^E \rangle + \frac{1}{4} \langle a_{\ell_1 m}^{T*} a_{\ell'_1 m'}^{T*} \rangle \langle a_{\ell_2 m}^E a_{\ell'_2 m'}^E \rangle \\ &+ \frac{1}{4} \langle a_{\ell_1 m}^{T*} a_{\ell'_2 m'}^E \rangle \langle a_{\ell_2 m}^E a_{\ell'_1 m'}^{T*} \rangle, \end{aligned} \quad (\text{D.8})$$

leading to

$$\begin{aligned} \frac{1}{4} \langle a_{\ell_1 m}^{T*} a_{\ell_2 m}^E a_{\ell'_1 m'}^{T*} a_{\ell'_2 m'}^E \rangle &= \frac{1}{4} \delta_{\ell_1 \ell_2} \delta_{\ell'_1 \ell'_2} C_{\ell_1}^{TE} C_{\ell'_2}^{TE} + \frac{1}{4} \delta_{\ell'_2 \ell_2} \delta_{\ell_1 \ell'_1} \delta_{m - m'} C_{\ell_1}^{TT} C_{\ell'_2}^{EE} + \\ &\frac{1}{4} \delta_{\ell_1 \ell'_2} \delta_{\ell_2 \ell'_1} \delta_{mm'} C_{\ell_1}^{TE} C_{\ell'_2}^{TE}, \end{aligned} \quad (\text{D.9})$$

similarly, the other terms in eq. D.7 will generate the following respective expressions

$$\begin{aligned} \frac{1}{4} \langle a_{\ell_1 m}^{T*} a_{\ell_2 m}^E a_{\ell'_1 - m'}^{T*} a_{\ell'_2 - m'}^E \rangle &= \frac{1}{4} \delta_{\ell_1 \ell_2} \delta_{\ell'_1 \ell'_2} C_{\ell_1}^{TE} C_{\ell'_2}^{TE} + \frac{1}{4} \delta_{\ell'_2 \ell_2} \delta_{\ell_1 \ell'_1} \delta_{mm'} C_{\ell_1}^{TT} C_{\ell'_2}^{EE} + \\ &\frac{1}{4} \delta_{\ell_1 \ell'_2} \delta_{\ell_2 \ell'_1} \delta_{m - m'} C_{\ell_1}^{TE} C_{\ell'_2}^{TE}, \end{aligned} \quad (\text{D.10})$$

$$\begin{aligned} \frac{1}{4} \langle a_{\ell_1 - m}^{T*} a_{\ell_2 - m}^E a_{\ell'_1 m'}^{T*} a_{\ell'_2 m'}^E \rangle &= \frac{1}{4} \delta_{\ell_1 \ell_2} \delta_{\ell'_1 \ell'_2} C_{\ell_1}^{TE} C_{\ell'_2}^{TE} + \frac{1}{4} \delta_{\ell'_2 \ell_2} \delta_{\ell_1 \ell'_1} \delta_{mm'} C_{\ell_1}^{TT} C_{\ell'_2}^{EE} + \\ &\frac{1}{4} \delta_{\ell_1 \ell'_2} \delta_{\ell_2 \ell'_1} \delta_{-mm'} C_{\ell_1}^{TE} C_{\ell'_2}^{TE}, \end{aligned} \quad (\text{D.11})$$

$$\begin{aligned} \frac{1}{4} \langle a_{\ell_1 - m}^{T*} a_{\ell_2 - m}^E a_{\ell'_1 - m'}^{T*} a_{\ell'_2 - m'}^E \rangle &= \frac{1}{4} \delta_{\ell_1 \ell_2} \delta_{\ell'_1 \ell'_2} C_{\ell_1}^{TE} C_{\ell'_2}^{TE} + \frac{1}{4} \delta_{\ell'_2 \ell_2} \delta_{\ell_1 \ell'_1} \delta_{m - m'} C_{\ell_1}^{TT} C_{\ell'_2}^{EE} + \\ &\frac{1}{4} \delta_{\ell_1 \ell'_2} \delta_{\ell_2 \ell'_1} \delta_{-m' - m} C_{\ell_1}^{TE} C_{\ell'_2}^{TE}. \end{aligned} \quad (\text{D.12})$$

Using the conditions stated in equation B.14 and getting the other part of the variance as  $\langle f_{\ell_1 \ell_2 m} \rangle \langle f_{\ell'_1 \ell'_2 m'} \rangle_{0th} = \delta_{\ell_1 \ell_2} \delta_{\ell'_1 \ell'_2} C_{\ell_1}^{TE} C_{\ell'_2}^{TE}$ , the result is

$$\sigma_{\ell_1 \ell_2 m}^2 = \frac{1}{2} \delta_{\ell_2 \ell'_2} \delta_{\ell_1 \ell'_1} (\delta_{m0} + 1) C_{\ell_1}^{TT} C_{\ell'_2}^{EE}. \quad (\text{D.13})$$

**Acknowledgments.** PSF thanks FAPES (Brazil) and FINEP/FACC (contract 01.22.0505.00) for financial support.

## References

- [1] **Simons Observatory** Collaboration, M. Abitbol et al., *The Simons Observatory: Science Goals and Forecasts for the Enhanced Large Aperture Telescope*, [arXiv:2503.00636](#).
- [2] A. MacInnis, N. Sehgal, and M. Rothermel, *Cosmological parameter forecasts for a cmb-hd survey*, *Physical Review D* **109** (2024), no. 6 063527.
- [3] **Planck** Collaboration, N. Aghanim et al., *Planck 2018 results. V. CMB power spectra and likelihoods*, *Astron. Astrophys.* **641** (2020) A5, [[arXiv:1907.12875](#)].
- [4] S. Owusu, Ferreira, P. da S., A. Notari, and M. Quartin, *The CMB cold spot under the lens: ruling out a supervoid interpretation*, *JCAP* **06** (2023) 040, [[arXiv:2211.16139](#)].
- [5] P. Vielva, E. Martinez-Gonzalez, R. B. Barreiro, J. L. Sanz, and L. Cayon, *Detection of non-Gaussianity in the WMAP 1 - year data using spherical wavelets*, *Astrophys. J.* **609** (2004) 22–34, [[astro-ph/0310273](#)].
- [6] M. Cruz, E. Martinez-Gonzalez, P. Vielva, and L. Cayon, *Detection of a non-gaussian spot in wmap*, *Mon. Not. Roy. Astron. Soc.* **356** (2005) 29–40, [[astro-ph/0405341](#)].
- [7] M. Cruz, M. Tucci, E. Martinez-Gonzalez, and P. Vielva, *The non-gaussian cold spot in wmap: significance, morphology and foreground contribution*, *Mon. Not. Roy. Astron. Soc.* **369** (2006) 57–67, [[astro-ph/0601427](#)].
- [8] M. Cruz, E. Martinez-Gonzalez, P. Vielva, J. M. Diego, M. Hobson, and N. Turok, *The CMB cold spot: texture, cluster or void?*, *Mon. Not. Roy. Astron. Soc.* **390** (2008) 913, [[arXiv:0804.2904](#)].
- [9] **Planck** Collaboration, P. A. R. Ade et al., *Planck 2015 results. XVI. Isotropy and statistics of the CMB*, *Astron. Astrophys.* **594** (2016) A16, [[arXiv:1506.07135](#)].
- [10] P. Vielva, *A comprehensive overview of the cold spot*, *Advances in Astronomy* **2010** (2010), no. 1 592094.
- [11] M. Cruz, E. Martinez-Gonzalez, and P. Vielva, *The wmap cold spot*, *arXiv preprint arXiv:0901.1986* (2009).
- [12] M. Cruz, M. Tucci, E. Martinez-Gonzalez, and P. Vielva, *The non-gaussian cold spot in wilkinson microwave anisotropy probe: significance, morphology and foreground contribution*, *Monthly Notices of the Royal Astronomical Society* **369** (2006), no. 1 57–67.
- [13] D. G. Lambas, F. K. Hansen, F. Toscano, H. E. Luparello, and E. F. Boero, *The cmb cold spot as predicted by foregrounds around nearby galaxies*, *Astronomy & Astrophysics* **681** (2024) A2.
- [14] **Planck** Collaboration, Planck Collaboration IV, *Planck 2018 results. IV. Diffuse component separation*, *Astron. Astrophys.* **641** (2020) A4, [[arXiv:1807.06208](#)].
- [15] Planck Collaboration, “FFP10: Full Focal Plane simulations of the Planck mission.” Planck Legacy Archive, ESA, 2019. <https://pla.esac.esa.int>.
- [16] H. Georgi and S. L. Glashow, *Unity of all elementary-particle forces*, *Physical Review Letters* **32** (1974), no. 8 438.
- [17] A. Vilenkin, A. Vilenkin, and E. Shellard, *Cosmic strings and other topological defects*. Cambridge University Press, 1994.
- [18] T. W. Kibble, *Topology of cosmic domains and strings*, *Journal of Physics A: Mathematical and General* **9** (1976), no. 8 1387.
- [19] N. Turok, *Global texture as the origin of cosmic structure*, *Physical Review Letters* **63** (1989), no. 24 2625.
- [20] S. Das and D. N. Spergel, *CMB Lensing and the WMAP Cold Spot*, *Phys. Rev. D* **79** (2009) 043007, [[arXiv:0809.4704](#)].

- [21] M. Farhang and M. S. Movahed, *CMB Cold Spot in the Planck light*, *Astrophys. J.* **906** (2021), no. 1 41, [[arXiv:2001.03995](#)].
- [22] I. Masina and A. Notari, *The Cold Spot as a Large Void: Lensing Effect on CMB Two and Three Point Correlation Functions*, *JCAP* **07** (2009) 035, [[arXiv:0905.1073](#)].
- [23] I. Masina and A. Notari, *Detecting the Cold Spot as a Void with the Non-Diagonal Two-Point Function*, *JCAP* **09** (2010) 028, [[arXiv:1007.0204](#)].
- [24] P. Vielva, E. Martínez-González, M. Cruz, R. B. Barreiro, and M. Tucci, *Cosmic microwave background polarization as a probe of the anomalous nature of the cold spot*, *Monthly Notices of the Royal Astronomical Society* **410** (Jan., 2011) 33–38, [[arXiv:1002.4029](#)].
- [25] K. Sousa and J. Urrestilla, *Cmb anisotropies by collapsing textures*, in *Progress in Mathematical Relativity, Gravitation and Cosmology: Proceedings of the Spanish Relativity Meeting ERE2012, University of Minho, Guimarães, Portugal, September 3-7, 2012*, pp. 409–413, Springer, 2013.
- [26] M. Cruz, N. Turok, P. Vielva, E. Martinez-Gonzalez, and M. Hobson, *A Cosmic Microwave Background feature consistent with a cosmic texture*, *Science* **318** (2007) 1612–1614, [[arXiv:0710.5737](#)].
- [27] M. Cruz, N. Turok, P. Vielva, E. Martinez-Gonzalez, and M. Hobson, *A cosmic microwave background feature consistent with a cosmic texture*, *Science* **318** (2007), no. 5856 1612–1614.
- [28] R. Durrer, M. Heusler, P. Jetzer, and N. Straumann, *General relativistic textures and their interactions with matter and radiation*, *Nuclear Physics B* **368** (1992), no. 2 527–553.
- [29] N. Turok and D. Spergel, *Global Texture and the Microwave Background*, *Phys. Rev. Lett.* **64** (1990) 2736.
- [30] R. Durrer, M. Kunz, and A. Melchiorri, *Cosmic structure formation with topological defects*, *Phys. Rept.* **364** (2002) 1–81, [[astro-ph/0110348](#)].
- [31] **CMB-HD** Collaboration, S. Aiola et al., *Snowmass2021 CMB-HD White Paper*, [[arXiv:2203.05728](#)].
- [32] **Planck** Collaboration, P. A. R. Ade et al., *Planck 2013 results. XXV. Searches for cosmic strings and other topological defects*, *Astron. Astrophys.* **571** (2014) A25, [[arXiv:1303.5085](#)].
- [33] W. Hu, *Weak lensing of the CMB: A harmonic approach*, *Phys. Rev. D* **62** (2000) 043007, [[astro-ph/0001303](#)].
- [34] M. Kamionkowski, A. Kosowsky, and A. Stebbins, *Statistics of cosmic microwave background polarization*, *Physical Review D* **55** (1997), no. 12 7368.